© 2020. Published by The Company of Biologists Ltd | Development (2020) 147, dev191726. doi:10.1242/dev.191726

RESEARCH ARTICLE

Ontogenesis of the tear drainage system requires Prickle1-driven polarized basement membrane deposition

Dianlei Guo*, Jiali Ru*, Fuxiang Mao, Hong Ouyang, Rong Ju, Kaili Wu, Yizhi Liu and Chunqiao Liu‡

ABSTRACT

In terrestrial animals, the lacrimal drainage apparatus evolved to serve as conduits for tear flow; however, little is known about the ontogenesis of this system. Here, we define the anatomy of the fully formed tear duct in mice, characterize crucial morphogenetic events for the development of tear duct components and identify the site for primordial tear duct (PTD) initiation. We report that the PTD originates from the orbital lacrimal lamina, a junction formed by the epithelia of the maxillary and lateral nasal processes. We demonstrate that *Prickle1*, a key component of planar cell polarity signaling, is expressed in progenitors of the PTD and throughout tear duct morphogenesis. Disruption of *Prickle1* stalls tear duct elongation; in particular, the loss of basement membrane deposition and aberrant cytoplasmic accumulation of laminin are salient. Altered cell adhesion, cytoskeletal transport systems, vesicular transport systems and cell axis orientation in *Prickle1* mutants support the role of *Prickle1* in planar cell polarity. Taken together, our results highlight a crucial role of Prickle1-mediated polarized basement membrane secretion and deposition in PTD elongation.

KEY WORDS: Basement membrane, Ontogenesis, Planar cell polarity, Polarized deposition, Prickle1, Tear duct

INTRODUCTION

The main function of tear flow is to lubricate the ocular surface, preventing it from drying. Disruption of tear production or flow leads to an unhealthy ocular surface, including dry eye syndrome, which has a global prevalence ranging between 5 and 50% (Sanchez-Tena et al., 2019). In many tetrapods, the orbital glands and the excretory/drainage conduits coevolved to produce and passage tears over the ocular surface (Frame and Burkat, 2009). The excretory lacrimal system, or tear duct (TD), consisting of the lacrimal canaliculi (LC) and the nasolacrimal duct (NLD) canals, also has absorptive and secretory functions, possibly providing feedback in tear production (Paulsen et al., 2002a,b, 2016). Despite its importance, the drainage system remains largely unexplored.

Comparative studies have demonstrated considerable phylogenetic variations in tear drainage ducts (Tamarin and Boyde, 1977; Paulsen et al., 2002a; Rossie and Smith, 2007; Frame and Burkat, 2009; Nowack and Wöhrmann-Repenning, 2010; Rehorek et al., 2011, 2015). The human NLD is of ectodermal origin and starts to develop at approximately 5.5 weeks of gestation (de la Cuadra-Blanco et al., 2006). The epithelial maxillary and nasal processes form a lacrimal groove, which then pinches off as a solid cord extending towards both the orbital and nasal directions (de la Cuadra-Blanco et al., 2006). The rabbit NLD has many anatomical aspects similar to that of humans and is considered a suitable model for study of the human NLD (Paulsen et al., 2002a; Frame and Burkat, 2009). However, unlike humans, the rabbit NLD originates in the subcutaneous region of the lower eyelid and extends unidirectionally to the naris (Rehorek et al., 2011). Similar observations were reported for a rodent animal, the Mongolian gerbil (Rehorek et al., 2015). The mouse NLD is assumed to develop similarly to humans, based on a scanning electron microscopy study (Tamarin and Boyde, 1977). However, such a notion faces challenges in that both the mouse and Mongolian gerbil are taxonomical of Rodentia, evolutionarily much closer to rabbits than humans. Thus, an examination of the ontogeny of the mouse NLD should resolve this contradiction.

The TD along with other facial structures, lip, palate and nose develop as a result of fusion and transformation of the facial processes through coordinated cellular proliferation, migration and apoptosis (Lotz et al., 2006; Ferretti et al., 2011). During embryogenesis, the fusion of the maxillary process (mxp) with the lateral nasal (lnp) and medial nasal (mnp) processes gives rise to the lambdoidal three-way seam (mxp/lnp/mnp), which further shapes midface development (Tamarin and Boyde, 1977; Depew and Compagnucci, 2008). Failure in fusion of the facial processes leads to cleft lip with or without cleft palate (CL/P). Wnt and fibroblast growth factor (Fgf) signaling are important for epithelial fusion. Notably, the Pbx-Wnt-p63-Irf6 axis is crucial for lambdoidal seam formation by controlling epithelial apoptosis (Ferretti et al., 2011). Additional to the frontal lambdoid junction, the nasolacrimal groove (NLG) is also formed towards the orbit by mxp and external lnp (Tamarin and Boyde, 1977). In humans, the NLG invaginates horizontally to form the lacrimal lamina (LL) and subsequently hollows out, giving rise to the tear drainage system (de la Cuadra-Blanco et al., 2006; Lotz et al., 2006). In contrast to the profound knowledge of the molecular genetics of lambdoidal fusion and CL/P (Ferretti et al., 2011; Li et al., 2019), the developmental and genetic determinants of LL/NLG are still lacking.

Defects in the LC and NLD are seen in several syndromic diseases with known causal mutations (Kozma et al., 1990; van Genderen et al., 2000; Inan et al., 2006; Jadico et al., 2006a,b; Rohmann et al., 2006; Foster et al., 2014). Among these, mutations in FGF signaling components (FGF10, FGFR2 and FGFR3) cause hypoplasia of the NLD and lacrimal puncta, often with conjunctivitis as part of the lacrimo-auriculo-dento-digital (LADD) syndrome (Rohmann et al., 2006). Consistent with these findings, mutations in p63, a transcription factor upstream of FGF signaling, lead to disorders overlapping with the LADD, in which lacrimal outflow obstruction can occur with agenesis of the NLD

State Key Laboratory of Ophthalmology, Zhongshan Ophthalmic Center, Sun Yat-sen University, Guangzhou 510060, China.
*These authors contributed equally to this work

‡Author for correspondence (liuchunq3@mail.sysu.edu.cn)

C.L., 0000-0002-1513-0073

Handling Editor: Liz Robertson
Received 17 April 2020; Accepted 23 October 2020

Development (2020) 147, dev191726. doi:10.1242/dev.191726

and LC (Allen, 2014). Congenital nasolacrimal duct obstruction (CNLDO) is present in up to 20% of newborn infants (Wallace et al., 2006; Vagge et al., 2018) and it is conceivable that many more genetic and/or genetic risk factors are yet to be uncovered.

The Wnt/planar cell polarity (PCP) pathway plays key roles in the morphogenesis of diverse tissues (Guo et al., 2004; Wang et al., 2006; Yu et al., 2012). Particularly for tubulogenesis, tubular branching, elongation and migration require PCP-driven convergent extension (CE) (Bernascone et al., 2017; Kunimoto et al., 2017). A set of six proteins, including Prickle, Frizzled, Disheveled, Vangl, Diego and Flamingo, executes Wnt/PCP signaling to control cell polarity and oriented cell migration (Wallingford et al., 2002; Wallingford and Harland, 2002). Mutations in *Vangl*, *Frizzled*, *Prickle* and a non-core PCP component, protocadherin *Fat*, all cause malformed renal tubules (Saburi et al., 2008; Liu et al., 2014; Kunimoto et al., 2017). Because TD development is a process of tubulogenesis, we hypothesized that it requires Wnt/PCP signaling. To test our hypothesis, we investigated the full course of TD ontogenesis in mice and identified a crucial role for Prickle1 in TD elongation.

RESULTS

Anatomy of the mouse tear duct at postnatal day 1

To gain insights into the tear drainage system in mice, we first investigated mouse TD anatomy by performing 3D reconstruction at postnatal day (P)1, when both the lacrimal gland and TD start functioning (Ru et al., 2020). We used p63, an epithelial marker, to identify the duct epithelium. Background staining from the antibody also outlined craniofacial bones, offering useful positional references. Images of the entire TD were taken at 30 µm intervals and used for 3D reconstruction. An illustration of the full path of the TD is presented in Fig. 1A,B and Movie 1. TD traveled a circuitous mediolateral path starting from the nasal cavity (Fig. 1C-E). It descended from the nasal cavity passing through the premaxillary bones, then ascended at the maxillary bones and branched near the eyeball as superior and inferior lacrimal canaliculus (SLC and ILC, respectively) (Fig. 1A-E). The lumen shape of the TD varied with position on sections (Fig. 1F-J,F′-J′), and the path appeared to be defined by the arrangement of the premaxillary and maxillary bones and incisors (Movie 2). In the nasal/anterior half, the TD traveled along the internal wall of the premaxillary bone surrounding the incisor in a downward path (Fig. 1G,G′; Movie 2) until the premaxillary and maxillary junction (Fig. 1H,H′; Movie 2), where it ascended sharply in the lateral direction and bifurcated into the upper and lower eyelids near the canthi (Fig. 1H-J,H′-J′; Movie 2).

Crucial events for tear duct development

Following investigation of TD anatomy, we looked into TD development at a series of embryonic ages to identify crucial events. To facilitate locating the PTD, we adopted the terms NLG (nasolacrimal groove, to describe the mxp-lnp junction) and LL (lacrimal lamina, to describe the thickening NLG) used in human anatomy (de la Cuadra-Blanco et al., 2006) to guide the search for the mouse PTD. We started at embryonic day (E)11, an early time point when the NLG emerged (Tamarin and Boyde, 1977). NLG is reported to form the LL where the tear drainage system originates in humans (de la Cuadra-Blanco et al., 2006). On parasagittal sections, an E-cadherin-stained epithelial protrusion connecting with the prospective conjunctiva was identified as the presumptive PTD through examination of multiple sections (Fig. 2A-D; Fig. S1A). The location for the emerging PTD appeared to be where the lnp and mxp meet to give rise to the orbital/optic LL (Fig. 2A-D; Fig. S1A). A thin stalk from the narrowing LL connected a multipolar shape of the PTD mass with the conjunctiva at E11.5 and E12 (Fig. 2E-H; Fig. S1B). Both the conjunctival end of the stalk and the PTD cell mass underwent apoptosis (Fig. S1C,D). Additionally, the lateral and orbital extreme of the PTD appeared to separate into two cell masses, which are predicted to be the primordia of the future ILC and SLC (Fig. S1B). The anterior/nasal portion of the predicted PTD had already extended a considerable distance at this age but could not be visualized with the orbital PTD on the same section (see later). The early PTD development from E10.5 to E11.5 is summarized in Fig. S1E.

To determine the timing of when the PTD reaches target tissues, we first sectioned the mouse head coronally to determine when the NLD reached the nasal cavity. The NLD extended close to the nasal cavity but did not reach it at E13.5 (Fig. S2A-F). At E14, the NLD reached the nasal cavity and merged with the nasal epithelium (Fig. 2I-L). Because the mouse head positioned for sectioning was not completely symmetrical to the vertical axis, only one side of the NLD was shown. The opposite side was beyond the joining point of the NLD and nasal epithelium. We next prepared parasagittal sections to define the timing of when the canaliculi joins the conjunctiva. The inferior lacrimal canaliculus (ILC) joined the conjunctival epithelium at E14 (Fig. 2M-P) when the SLC still had a distance to reach the upper eyelid (Fig. S2G-I). By E16.5, both the ILC and the SLC had joined the conjunctival epithelium of the lower (Fig. 2Q-T) and upper eyelid (Fig. 2U-X), respectively. Thus, the data demonstrate that the early TD connects with the conjunctiva epithelium and completely reaches target tissues by E16.5.

Initiation of the PTD from the orbital LL of the NLG

To track the first PTD emergence, we first performed 3D reconstruction on early embryos of several ages from E10.25 to E11. Development of the facial primordia begins around E9.5∼E10.5, with the hallmark of a lambdoidal junction at the midface formed by the fusion of the mxp with the medial and lateral nasal processes (mnp and lnp; Fig. 3A) (Tamarin and Boyde, 1977; Ferretti et al., 2011). Within a similar time window, lateral expansion of the mxp towards the orbit results in a nasolacrimal groove (NLG) and its derived lacrimal lamina (LL) between the mxp and lnp (Tamarin and Boyde, 1977), giving rise to the TD system in humans (de la Cuadra-Blanco et al., 2006). 3D reconstruction of parasagittal E-cadherin-stained sections at ∼E10.25 did not show an obvious PTD viewed from different perspectives, but a thickening lamina proximal to the orbit (Fig. 3A-C; Movie 3). This lamina structure is predicted to be equivalent to the human LL, which is formed by the coalesced mxp and lnp (de la Cuadra-Blanco et al., 2006). Parasagittal sections demonstrated a deep ingress of the predicted LL towards the orbit from the lateral to medial NLG (Fig. 3D-F). A few cells spreading out from the edge of the LL were suspected to be PTD precursors (Fig. 3F). At E10.5, using p63 immunolabeling with tissue clearance (Renier et al., 2014), both reconstructed 3D images and single sections demonstrated budding of the PTD from the edge of LL (Fig. 3G-L; Movies 4,5). Similar observations were made for the E11 PTD except that it extended farther (Fig. 3M-S; Movies 6,7). Taken together, the data extends and differs from the results of a previous human study, which will be discussed later.

Prickle1 expression coincided with and continued through the tear duct elongation

We next used *in situ* hybridization to investigate whether Wnt/PCP signaling components, which play essential roles in tubulogenesis

Development (2020) 147, dev191726. doi:10.1242/dev.191726

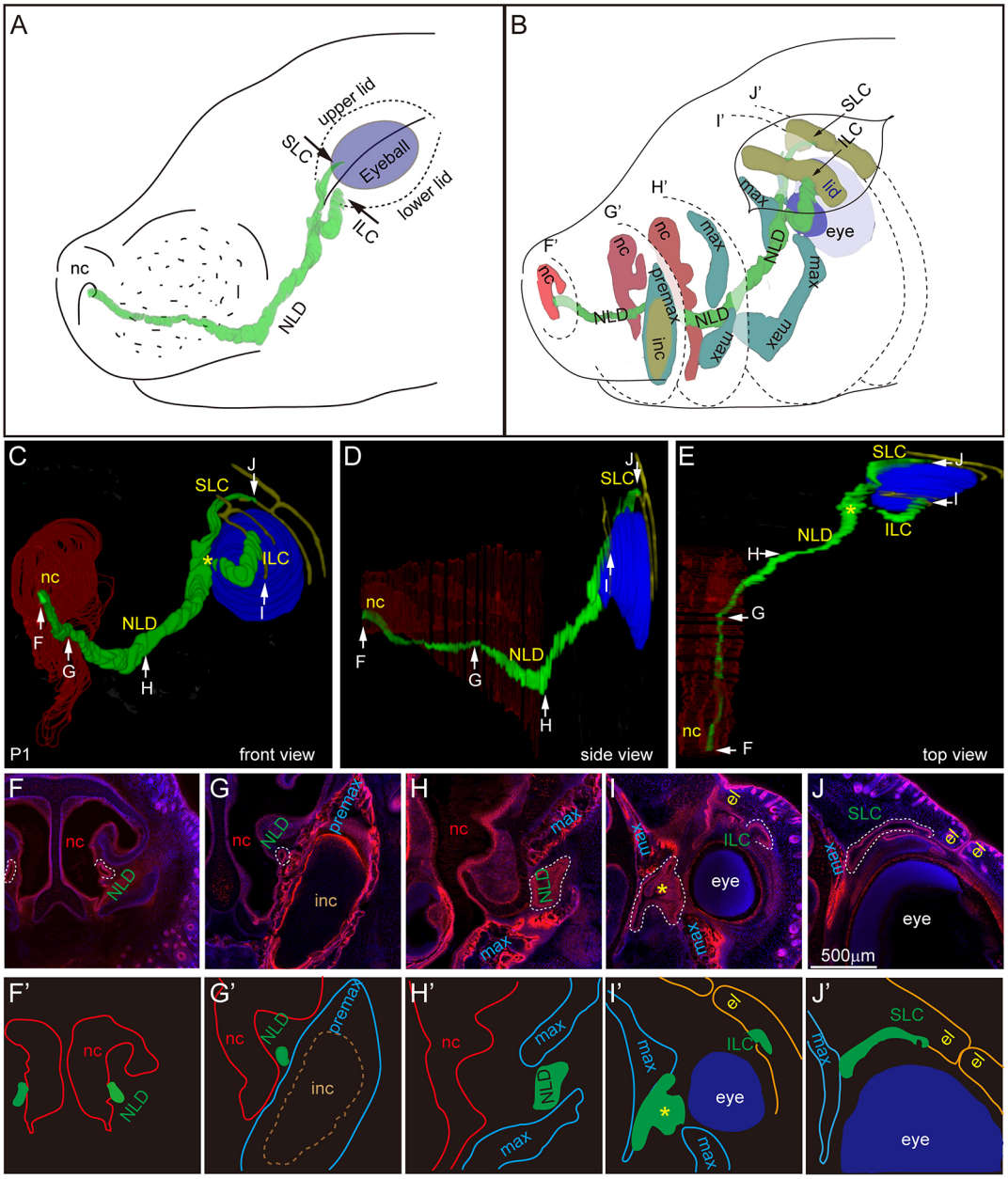

Fig. 1. 3D reconstruction of the P1 tear duct from p63 stained images. Four mice were examined for TD path on sections, all demonstrating the same TD anatomy. One was used for 3D reconstruction. (A,B) Drawings of the reconstructed P1 TD within the mouse head. Cutting planes and reference marks in B correspond to F-J and F′-J′. (C-E) Front (C), side (D) and top (E) views of the reconstructed P1 TD. Arrows with letters F-J correspond to images F-J and schemes F′-J′. The TD is filled with green. Asterisks indicate joining of the SLC and ILC. el, eyelid; ILC, inferior canaliculus; inc, incisor; max, maxillary bones; nc, nasal cavity; NLD, nasolacrimal duct; premax, premaxillary bone; SLC, superior canaliculus.

in a variety of tissues, were expressed in PTD. A number of Wnt/PCP genes were expressed in the developing TD (Ru et al., 2020). Among these, *Prickle1* is expressed exclusively in the PTD but not in the conjunctival epithelium. Taking advantage of a knock-in eYFP reporter in the *Prickle1* heterozygous null allele (Liu et al., 2013), we first examined whether *Prickle1* was expressed during PTD initiation. On serial consecutive sections at E10.25 (when the PTD just emerges from the LL; Fig. 3A-F), *Prickle1* was expressed in the facial primordium at high levels in the nasal process and at medium levels in the mxp mesenchyme and epithelium (Fig. 4A-I). A few cells from the orbital end of the LL/NLG with low-level expression of E-cadherin were predicted to be the PTD anlage without considerable *Prickle1* expression (Fig. 4G,I). At E10.5 (Fig. 4J-R), *Prickle1* expression was distinctly enhanced in the mxp epithelium of the NLG, with downregulation in the mesenchyme (Fig. 4L-P). Similar to the situation in E10.25, a group of E-cadherin-less cells budding or migrating from the orbital end of the LL/NLG showed moderate *Prickle1* expression, in contrast to the surrounding tissues (Fig. 4P,R). The lower level of E-cadherin staining in the budding cells might be a sign of epithelial-to-mesenchymal transition, which is involved in active cell migration. Together, these data suggest that *Prickle1* expression in the NLG mxp epithelium and budding PTD epithelial cells might have essential roles in PTD elongation rather than initiation.

We next investigated *Prickle1* expression in a series of ages of embryos during TD elongation. *Prickle1* was strongly expressed in

Development (2020) 147, dev191726. doi:10.1242/dev.191726

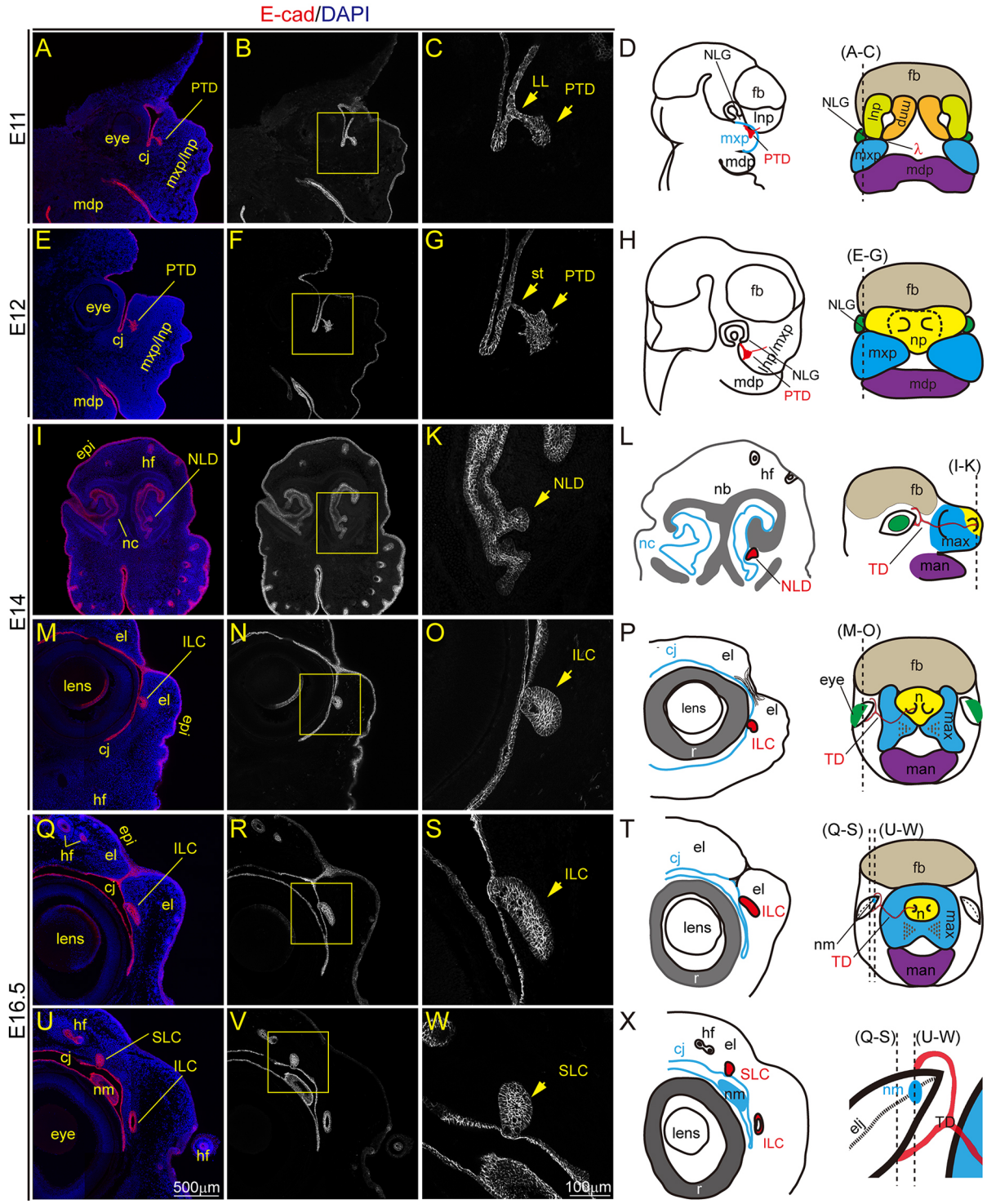

Fig. 2. Crucial events for drainage system development identified by E-cadherin staining. Three embryos of each age were examined for TD path on sections, all demonstrating consistent TD morphology. Representative sections from one embryo are demonstrated. (A) Parasagittal section of E11 mouse head showing the PTD. (B) Single E-cad channel from A. The boxed area in B is magnified in C. (D) Lateral (left) and frontal (right) views of E11 head. Dashed lines indicate the cutting position. (E-H) An E12 head section with the same treatment and arrangement as for A-C. (I-K) Frontal section of E14 head demonstrating nasolacrimal duct (NLD) fusing with the nasal cavity (nc) epithelium. (L) Left: Upper region of section I. Right: Lateral view of E14 embryonic head. (M-O) Inferior lacrimal canaliculus (ILC) fusing with the lower eyelid conjunctiva at E14 on a parasagittal section. (P) Left: Drawing of section M. Right: Frontal view of E14 head. (Q-T) ILC fusing with the lower eyelid conjunctiva at E16.5. Panels are arranged in the same way as for M-P. The nictitating membrane (nm), vestigial transparent third eyelid for moistening cornea while maintaining vision, is shown. (U-X) Superior lacrimal canaliculus (SLC) fusing with the upper eyelid at E16.5. Panels arrangement is same as Q-T, except that the right-hand drawing in X shows a zoomed-in location of the nasal canthus (nasal corner of the eye) from the right-hand drawing in T. λ, lambdoidal junction; cj, conjunctiva; el, eyelid; elj, eyelid junction; epi, epidermis; fb, forebrain; hf, hair follicles; lnp, lateral nasal process; man, mandible; max, maxilla; mdp, mandibular process; mnp, medial nasal process; mxp, maxillary process; mxp/lnp, joined mesenchyme of the maxillary and lateral nasal processes; n, nose; nb, nasal bone; nc, nasal cavity; NLG, nasolacrimal groove; nm, nictitating membrane; np, nasal plate.

Development (2020) 147, dev191726. doi:10.1242/dev.191726

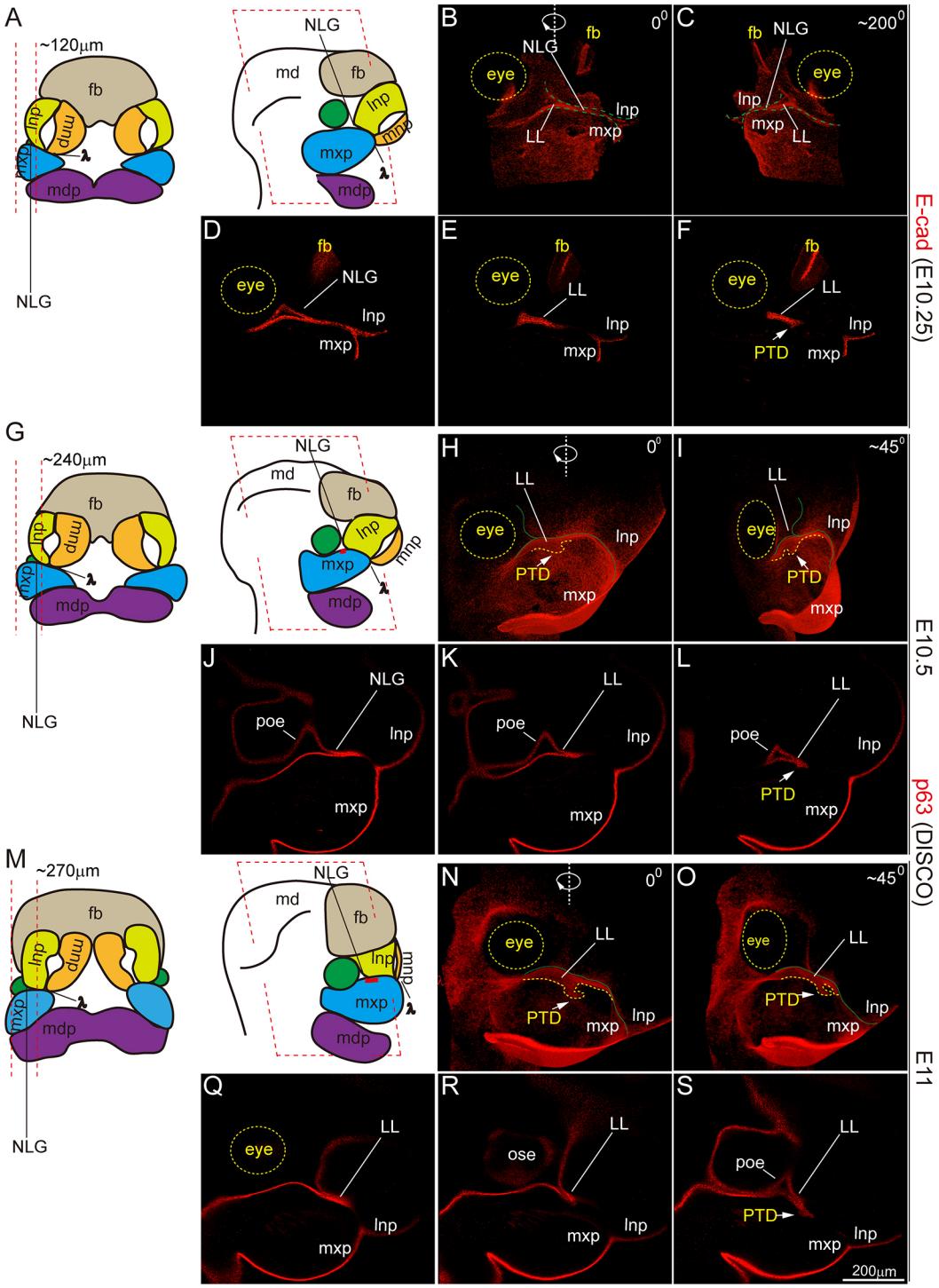

Fig. 3. Initiation of PTD from the orbital nasolacrimal groove at E10.25. Three embryos of each age were examined for PTD development by whole mount staining with E-cadherin, all demonstrating consistent spatiotemporal PTD initiation. (A) Diagrams of frontal (left) and lateral (right) views of an E10.25 head. Dashed lines indicate cutting positions and thickness in between for 3D reconstruction. (B,C) Inside view of reconstructed images at different angles. 0° in B is subjectively chosen to show key facial components. (C) Approximate 200° rotation around the *y*-axis, viewing the outside facial surface. Green dashed lines demarcate lnp and mxp junction of the NLG. (D-F) Three representative parasagittal sections from lateral to medial direction show geographical locations of the NLG and the lacrimal lamina (LL) relative to the lnp, mxp and other facial structures. (G-L) E10.5 embryos. Panels are arranged in the same way as for A-F, except that p63 was used as an epithelial marker for immunostaining with tissue clearance. Note the budding PTD from the LL (H,I). (M-S) E11 embryos. Panels are arranged in the same way as for G-L. md, midbrain; ose, ocular surface ectoderm; poe, periocular ectoderm; other abbreviations are as listed in Fig. 2.

the PTD cells near the orbit at E11 on parasagittal sections (Fig. 5A-D, green). On horizontal sections, *Prickle1* was strongly expressed in the frontal area of the nasal/maxillary processes, with moderate but distinct expression in the elongating PTD (Fig. 5E,F). Similar expression was found for E11.5 and E12 PTD (Fig. 5G-R) with downregulation in the frontal areas (Fig. 5K,L). Bifurcation of the canaliculi and the anterior NLD were clearly seen at E13 on separate parasagittal sections strongly expressing

Development (2020) 147, dev191726. doi:10.1242/dev.191726

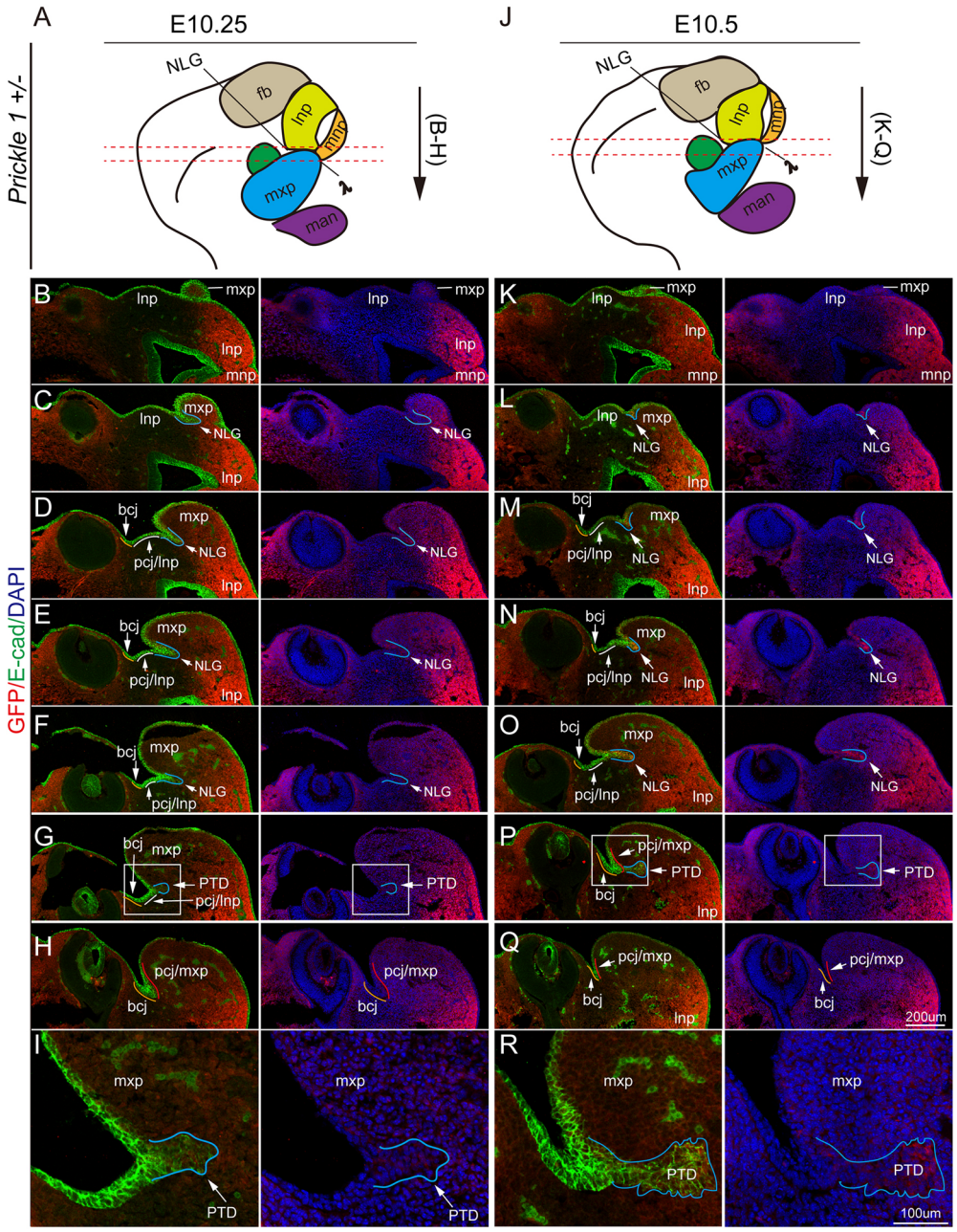

Fig. 4. Onset of *Prickle1* expression during tear duct development. Three embryos of each age were subjected to sectioning and immunostained with E-cadherin (green) and GFP reporter (red) for *Prickle1* gene. Images from one of these embryos for each age are presented. Blue, white, orange and red lines indicate the NLG, presumptive palpebral conjunctiva from the lateral nasal process (pcj/lnp), presumptive bulbar conjunctiva (bcj) and presumptive palpebral conjunctiva from the maxillary process (pcj/mxp), respectively. Note that the pcj/mxp is labeled only when mxp starts to merge with bcj; otherwise, mxp is used. (A) Diagram of lateral view of E10.25 head. Dashed lines indicate the sectioning region and orientation. Arrows indicate the sectioning direction. (B-H) Consecutive sections cutting through the NLG region at 30 µm. The left column shows merged channels for E-cadherin and GFP, and the right column shows merged channels for GFP and DAPI. (B) The mxp emerged on sections with weak mesenchymal *Prickle1* expression. (C) The mxp merged with lnp with enhanced mesenchymal *Prickle1* expression. (D-F) The enlarging mxp and appearance of the NLG. *Prickle1* was equally expressed in the mxp epithelium and mesenchyme. (G) PTD bud in conjunction with the prospective conjunctiva. Weak E-cadherin expression was observed in the PTD bud with *Prickle1* expression at background level. (H) The inner surface of the mxp started to merge with the prospective bulbar conjunctiva. (I) Magnification of the boxed area in G. (J) Diagram of E10.5 head. (K-Q) Sections are anatomically comparable to B-H. (K) The mxp emerged on sections. (L-O) *Prickle1* expression was conspicuously enhanced in a region of the mxp epithelium that becomes a part of NLG. (P) Distinct expression of *Prickle1* was detected in extending PTD with attenuated E-cadherin expression. (Q) The inner surface of the mxp merged with bulbar conjunctiva. (R) Magnification of the boxed area in P.

Prickle1 (Fig. 5T-Y), which continued until the LC and the NLD reached their target tissues (Fig. S3A-D). Thus, the combined expression data defines *Prickle1* as a bona fide marker for TD ontogenesis.

Disruption of *Prickle1* stalled tear duct outgrowth

The unique *Prickle1* expression pattern prompted us to query its function in TD development. Using *Prickle1* null mutants that were created previously (Liu et al., 2014), we first performed 3D

Development (2020) 147, dev191726. doi:10.1242/dev.191726

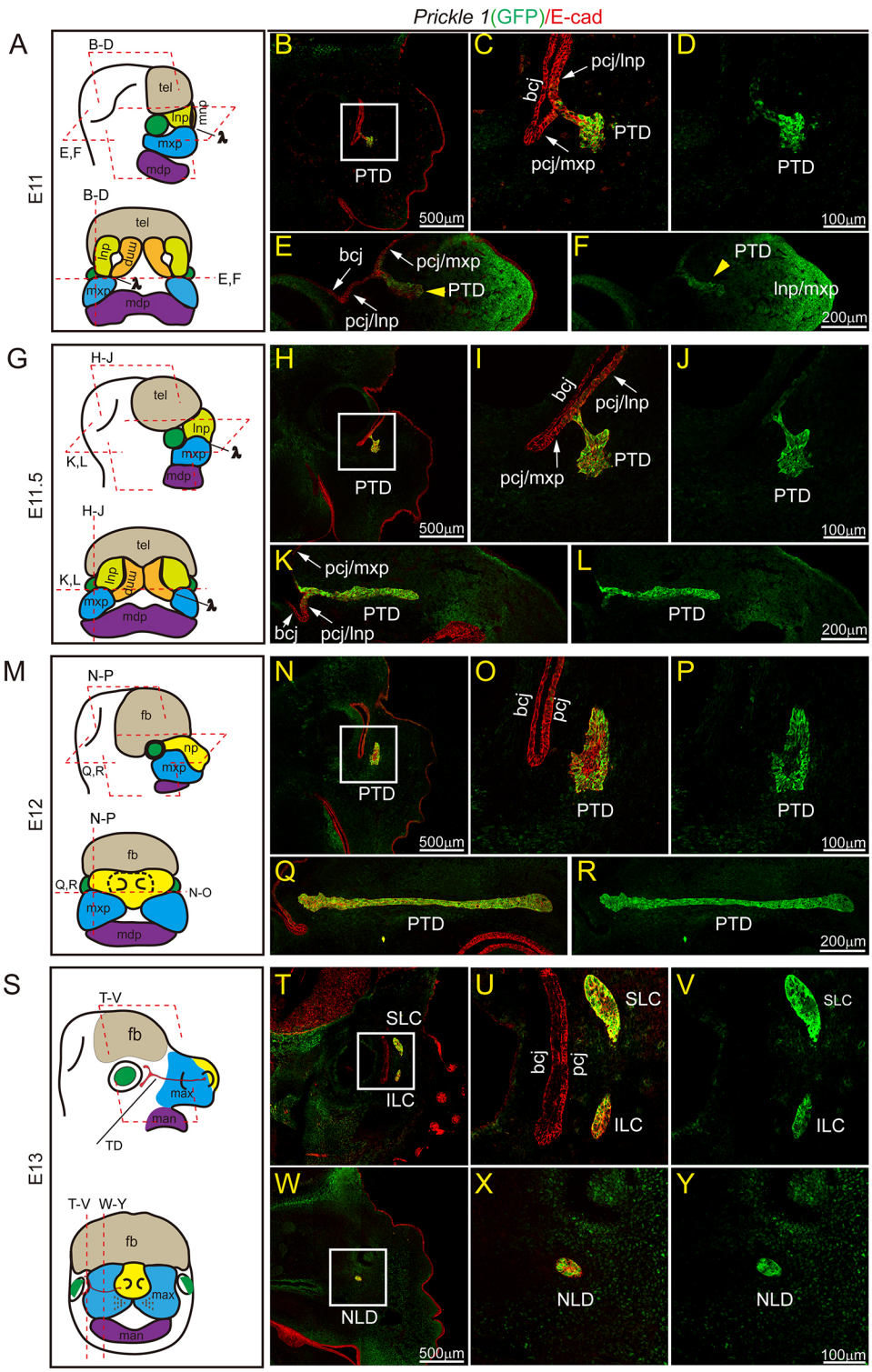

Fig. 5. Expression of *Prickle1* during tear duct elongation. Three embryos of each age were subjected to sectioning and immunostained with E-cadherin (red) and GFP reporter (green) for *Prickle1* gene. Images from one of these embryos for each age were presented. In all panels, *Prickle1* expression is indicated by a genetically knocked in *eYFP* reporter stained with anti-GFP antibody (green). E-cadherin marks general epithelium (red). Boxed areas are magnified in right panels of the same row. (A) Drawings of lateral (upper) and frontal (lower) views of E11 embryonic head with dashed lines and parallelograms indicating approximate cutting planes and positions for B-F. (B-D) Parasagittal section at E11 showing *Prickle*1 expression in the PTD epithelial cells. The boxed area in B is magnified in C (merged E-cadherin and GFP channels) and D (separate GFP channel). (E,F) Horizontal sections demonstrate the extending PTD with high *Prickle1* expression. (E) Image of merged E-cadherin and GFP channels. (F) Separate GFP channel. (G) Drawing of E11.5 embryonic head showing cutting planes and positions for H-L. (H-L) Images with the same arrangement as B-F. (M-R) E12 head and images with the same arrangement as A-F. (S) Drawings of E13 head as described in A. (T-Y) Parasagittal sections showing the SLC and ILC branches near to the orbital conjunctiva (T-V) and the advancing NLD (W-Y). Abbreviations are as described in previous figures.

reconstruction to monitor the progression of TD elongation in both wild-type and mutant embryos at half-day intervals from E11 to E14. This offered an additional opportunity to have an overall look at the full course of TD development. Consistent with previous observations (Figs 4,5), on lateral views, the wild-type tear duct anlage/PTD became conspicuous as early as E11 (Fig. 6A). As the PTD elongated, the anterior became thinner and advanced nasally, whereas the posterior became thickened with a narrow stalk connected to the original surface ectoderm (Fig. 6B,C). By E12.5, the PTD had completely separated from the surface ectoderm and was transformed into three tubular branches (Fig. 6D). The long anterior branch was the future NLD, and the shorter posterior branches were the prospective upper and lower canaliculi (SLC and ILC). The three tubules continued to grow towards their prospective targets, the conjunctival and the nasal epithelia (Fig. 6E-G). The whole tear drainage system – the canaliculi and the NLD – and its spatial relationship to the conjunctiva and the nasal cavity was clearly recognizable after E12.5 (Fig. 6E-G).

Development (2020) 147, dev191726. doi:10.1242/dev.191726

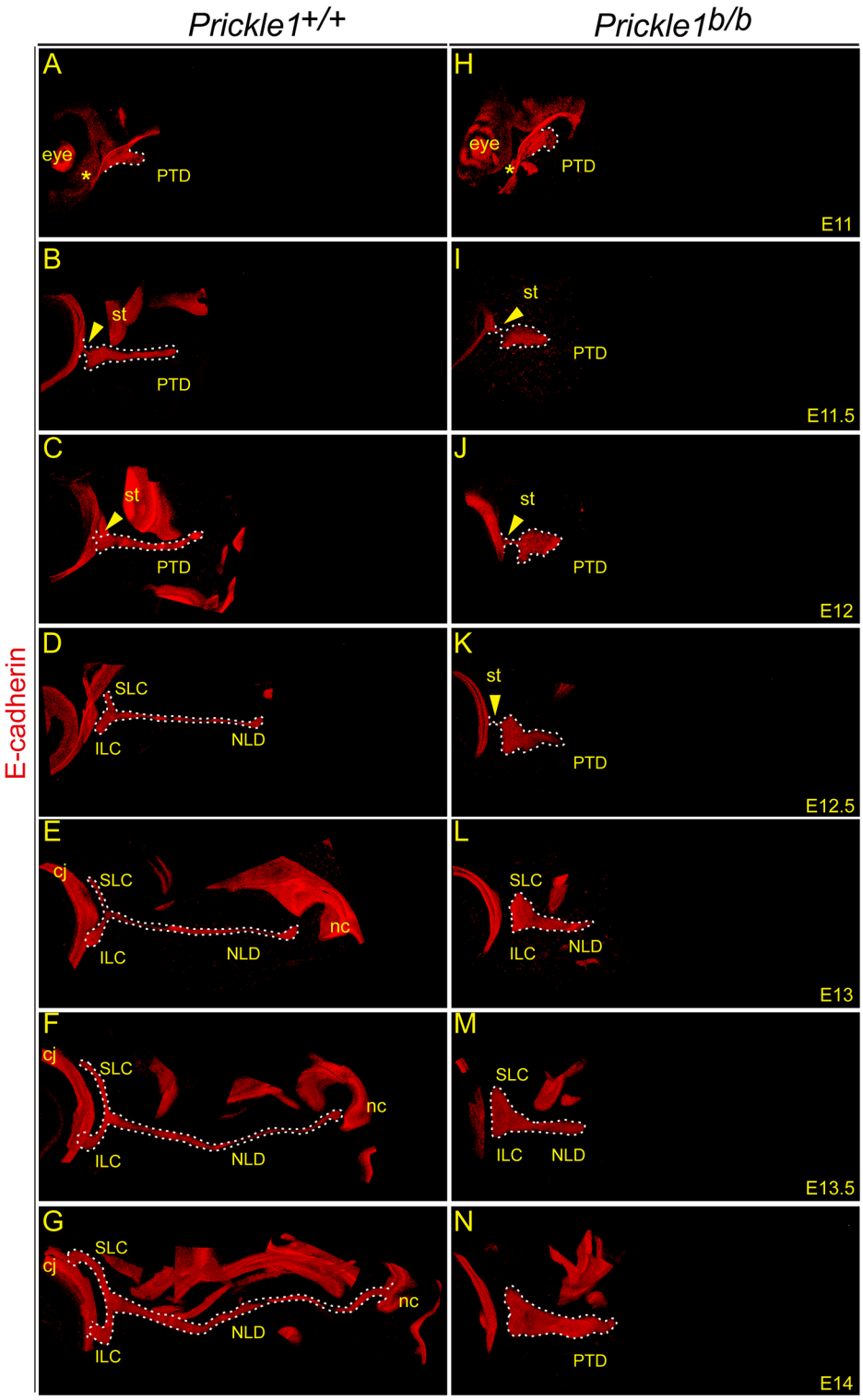

Fig. 6. Disruption of *Prickle1* stalls tear duct outgrowth. Three embryos of each age were examined for PTD development on vibratome sections (100 µm) stained with E-cadherin followed by 3D reconstruction. All embryos from each genotype demonstrated a consistent PTD growth pattern. 3D-reconstructed PTD from one embryo for each genotype and embryonic age is presented as a side view. (A-G) The developing wild-type TD system at serial embryonic ages. Note the connecting stalk (arrows) at E11.5 (B) and E12 (C) and the branches for prospective canaliculi at E12.5 (D). (H-N) The mutant TDs at the same ages as the wild type, showing shortened and broadened features. Arrows point to the connecting stalks. cj, conjunctiva; st, stalk. Dotted lines outline the PTD, whereas the asterisks indicate prospective conjunctiva.

The mutant PTD was similarly initiated as the wild type at E11 (Fig. 6H); however, it was shorter and wider at all later ages examined (Fig. 6I-N). Separation of the epithelial stalk from the presumptive conjunctiva was accomplished at E13 (Fig. 6L), half a day later than that of the wild type, which was complete at E12.5 (Fig. 6D). Collective movement or migration of the outgrowing epithelial cells was hampered (Fig. 6I-N), and characteristics of the LC and NLD branches were barely identifiable in the mutants (Fig. 6K-N). Thus, ablation of *Prickle1* stalled TD outgrowth, which is consistent with its expression in this organ.

Disruption of *Prickle1* impaired cell-cell adhesion and polarized basement membrane secretion

To examine cellular changes in the mutant PTD, we first examined E-cadherin/catenin junction complexes on horizontal sections of E11.5 embryos. β-Catenin and E-cadherin were normally

Development (2020) 147, dev191726. doi:10.1242/dev.191726

colocalized at the cell junction throughout the PTD (Fig. 7C-E; Fig. S4C,D,G,H). In mutants, however, β-catenin was mostly localized in the cytoplasm, and E-cadherin staining was patchy rather than continuous (Fig. 7F-H; Fig. S4E,F,I,J). Notably, the proximal mutant PTD often had relatively normal cell junctions in comparison with other areas (Fig. 7F–H). Further examination of α- and p120 catenins revealed a regional difference for their localization, in that the advancing tip in wild-type mice exhibited more cytoplasmic staining than the rest of the tube (Fig. S4K,L,S,T). This regional difference also existed in basement membrane (BM) components (see later). Regardless, like β-catenin, both α- and p120 catenins were ectopically located in the cytoplasm throughout the mutant duct along with patchy E-cadherin in the majority of areas (Fig. S4M,N,Q,R,U,V,Y,Z). Additionally, the broadened and shortened mutant PTD appeared to have massive loosely connected cells in the presumptive lumen (Fig. 7F-H; Fig. S4).

The accumulation of luminal cells in the mutant PTD suggested defective cell-matrix adhesion, which could be simply due to the absence of BM. Examination of extracellular matrix (ECM) proteins in the BM confirmed this hypothesis. In the wild type, BM components were deposited to the basal lamina (Fig. 7I,K,O,P) and displayed a notable loss in the advancing tip area of the PTD (Fig. S5D,J,P). In mutants, laminin, collagen IV and Perlecan were all mislocalized and the BM was disrupted in all areas but the initial stalk (Fig. 7L,N,R,S). A considerable amount of laminin was trapped in the mutant cytoplasm along with the integrin α-6 receptor (Fig. 7L-N). Collagen IV and Perlecan were secreted ectopically on the presumptive lumen/apical side (Fig. 7R,S). Interestingly, the basal localization of fibronectin was largely preserved throughout the mutant PTD (Fig. 7Q,T). Taken together, results show that both cell-cell and cell-matrix adhesions were disrupted in the mutant PTD.

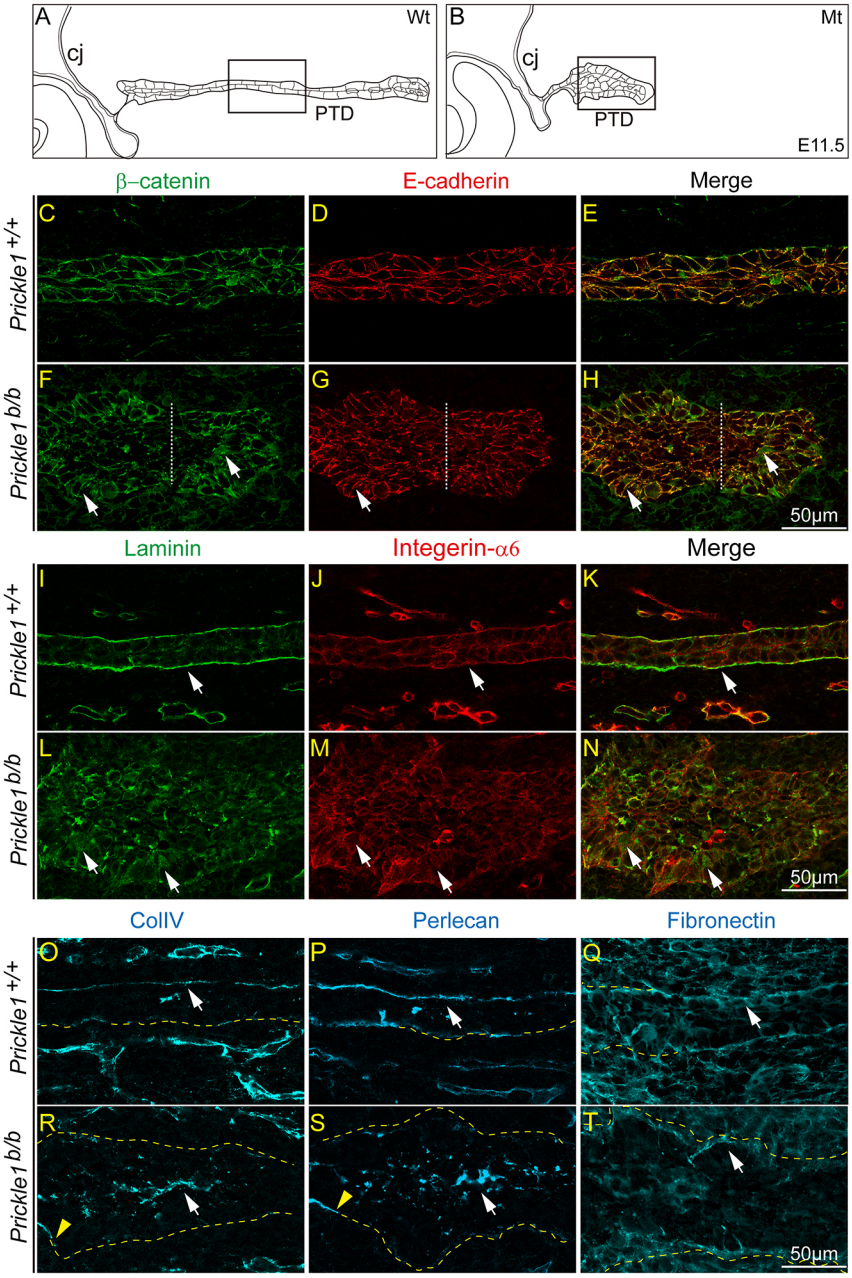

Fig. 7. Disruption of *Prickle1* impairs cell-cell and cell-matrix adhesion. Three embryos of each genotype were subjected to preparation of frozen sections and immunostaining, and all demonstrated consistent labeling. A set of images from one embryo for each genotype is displayed. (A,B) Illustration of the developing TD at E11.5 in the wild type (A) and *Prickle1* mutant (B). Boxed areas in A and B roughly correspond to regions shown in images of wild-type and mutant ducts, respectively. (C-H) Tissue sections co-labeled with β-catenin (green) and E-cadherin (red). Dashed lines roughly divide anterior/orbital and posterior/nasal halves of the PTD in the mutants. Arrows within posterior halves of the PTD in F-H indicate relative normal localization of β-catenin and E-cadherin in the mutants, whereas arrows within the anterior halves indicate cytoplasmic β-catenin localization. (I-N) Tissue sections co-labeled with laminin (green) and integrin-α6 (red). Arrows in wild-type tube (I-K) point to basal deposition of laminin and integrin-α6 receptor, and indicate cytoplasmic localization of laminin and integrin-α6 (L-N) in mutants. (O,R) Collagen IV basal deposition in wild-type PTD (O, white arrow) becomes mostly luminal in the mutant (R, white arrow). The yellow arrowhead points to the initial part of the mutant PTD with normally deposited basement membrane. (P,S) Perlecan deposition was essentially the same as collagen IV in both wild type and mutants. (Q,T) A similar basal deposition of fibronectin was observed in both wild type (Q) and the mutant PTD (T). Yellow dashed lines outline the PTD contours.

Development (2020) 147, dev191726. doi:10.1242/dev.191726

Disruption of *Prickle1* altered cytoskeleton and vesicle compartments

The endoplasm-trapped and ectopically secreted BM components in mutant PTD cells led us to further examine the cytoskeletal organization, which is directly involved in secretory pathways. The massively disorganized mutant luminal cells prevented us from gathering information comparable with that of the wild type; thus, we only examined the duct wall cells. Heavily stained actin bundles were observed in both wild-type and mutant PTD at E11.5 (Fig. 8A-D). However, actin filaments in the mutants appeared less packed and often formed spikes crossing the tissue boundary (Fig. 8B,D). Apical actin fibers overlying horizontally on the free lumen surface were often found in wild-type PTD (Fig. 8A,C), but were rarely distinguishable in the mutant (Fig. 8B). Similarly, horizontally run stable microtubule tracks in the wild type, labeled with acetylated α-tubulin, were not detected in mutants (Fig. 8E-H).

Because vesicle trafficking on microtubules and actin fibers directs proteins to different secretory pathways, we examined whether the endoplasmic compartments in the mutant PTD were also affected. Examination of endocytic vesicles showed that the majority of clathrin-coated endosomes were localized along the apical domain of wild-type PTD (Fig. 8I,K), but were considerably expanded along the apicobasal axis in the mutant (Fig. 8J,L). In contrast, in terms of localization, the Golgi complex appeared grossly normal in mutants (Fig. 8N,P compared with Fig. 8M,O). We also measured the cell axis and division orientations, which are key features of planar cell polarity, referring to the direction of PTD extension. The axis and division orientations indicated by the Golgi complex and acetylated tubulin, respectively, were both randomized in mutants (Fig. 8Q,R). These data are consistent with the observed protein trafficking defects of BM components in the *Prickle1* mutant.

DISCUSSION

Scant attention has been paid to development of the tear drainage system despite its importance. A few studies have focused primarily on comparative anatomy between species (Paulsen et al., 2002a; de la Cuadra-Blanco et al., 2006; Frame and Burkat, 2009; Rehorek et al., 2011). The current study details the ontogenesis of the mouse tear drainage system and outlines several crucial events: TD origin, elongation and reaching of final destinations. The study provides genetic and molecular insights into TD tubulogenesis, highlighting polarized BM secretion controlled by Prickle1 as a crucial mechanism for duct elongation.

To date, only one group has described the ontogenesis of the mammalian excretory lacrimal system by observing human embryos at the early stages (de la Cuadra-Blanco et al., 2006). This study concludes that separation of the LL of the NLG from the surface ectoderm to form a lacrimal cord is the primordium of the tear drainage system. However, it remains unclear where and how

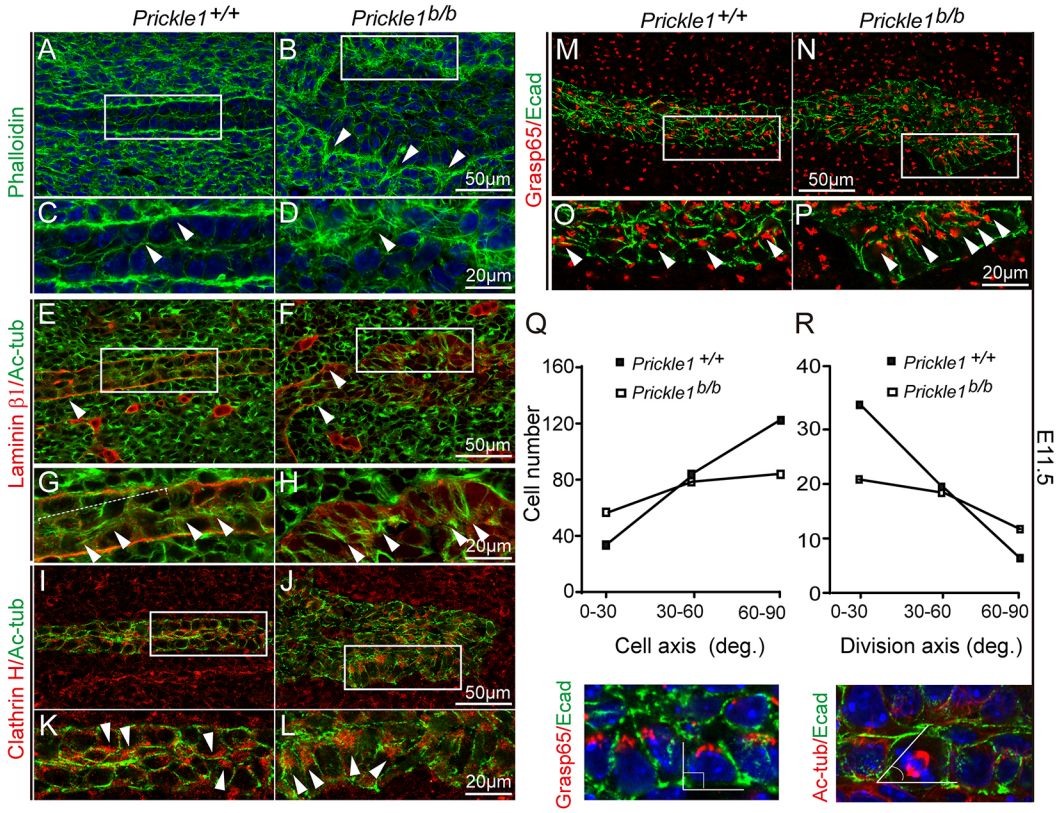

Fig. 8. Disruption of *Prickle1* alters cytoskeleton and vesicle compartments. Three embryos of each genotype were subjected to preparation of frozen sections and immunostaining, and all demonstrated consistent labeling. A set of images from one embryo for each genotype is displayed. Each boxed area is magnified in the corresponding panel below. (A-D) Phalloidin staining of actin filaments. Arrowheads point to actin bundles. (E-H) Acetylated α-tubulin (green) and laminin β1 (red) staining. Arrowheads in E and F point to the basement membrane labeled by laminin β1 (red). Arrowheads in G and H point to orientated microtubule tracks. (I-L) Clathrin and E-cadherin staining. Arrowheads point to apically distributed vesicles. (M-P) Grasp 65 staining. Arrowheads point to apically stained cis-Golgi cisternae. (Q) Quantification of cell axis orientation using Grasp 65 and E-cadherin to define apicobasal axes. A total of 236 wild-type and 215 mutant cells from 4 animals of each genotype were quantified. (R) Quantification of cell division orientation using acetylated α-tubulin and E-cadherin to define division angles. A total of 61 wild-type and 53 mutant cells from 8 animals for each genotype were quantified.

Development (2020) 147, dev191726. doi:10.1242/dev.191726

the LL detaches from the surface ectoderm to become the drainage system. The current study makes several distinct findings: (1) PTD outgrows from orbital invagination of the LL, which is contiguous with the presumptive palpebral conjunctiva of the eyelid folds that are formed by mxp and lnp epithelia. (2) As the PTD grows, the initially broad LL narrows to a stalk and eventually detaches from the conjunctiva epithelium, probably through apoptosis. (3) PTD branching to make the canaliculi appears to start at about E11.5, forming two separating cell masses at the orbital extreme of the PTD. (4) PTD progenitors appear to be those of *Prickle1*-expressing mxp epithelial cells, which constitute and later grow out from the LL. Both the mouse and human TDs initiate from the LL/NLG. However, LL thickening in humans appears near the frontal area where the mxp coalesces with the lnp and mnp (de la Cuadra-Blanco et al., 2006), namely, the lambdoidal junction in mice (Tamarin and Boyde, 1977; Ferretti et al., 2011). This contrasts with mice in that the initiating PTD is at the orbital edge of the LL.

The PTD progenitors in the LL appear from the mxp epithelium cells preferentially expressing *Prickle1*. Part of the conjunctiva also developed from the mxp. The conjunctiva consists of the palpebral and bulbar conjunctiva. In human studies, the palpebral conjunctiva is the inner surface of the eyelids, which are extensions of the mxp (for lower eyelid) and nasal plate (for upper eyelid) surface ectoderm (Pearson, 1980; Sevel, 1988; Byun et al., 2011; Tawfik et al., 2016). A literature search did not find similar statements for mouse eyelid development. However, the similar topographical arrangement of the facial processes in humans and mice, particularly the apparent folding of the mxp and lnp over the eyeball surface, predicts that the mouse eyelid and palpebral conjunctiva also originate from mxp and lnp. Thus, the mouse PTD and the palpebral conjunctiva of the lower lid are all of mxp origin, but from different regions.

The mouse PTD initially connects with the conjunctiva through the LL of the NLG, which later separates from it and branches into the primordium of the lacrimal canaliculi. The developing canaliculi later reconnects to the conjunctiva of the upper and lower eyelids to serve as drainage conduits. From an evolutionary perspective, why initially connected tear drainage system and conjunctiva undergo separation and reconnection during development remains to be addressed. Additionally, comparative studies indicate considerable phylogenetic variation in the development of drainage ducts. For instance, the rabbit NLD originates in the subcutaneous region of the lower eyelid, extending unidirectionally to the naris (Rehorek et al., 2011) similar to that of a rodent animal, the Mongolian gerbil (Rehorek et al., 2015). Surprisingly, although the mouse and Mongolian gerbil are both taxonomically Rodentia, evolutionarily closer compared with the rabbit, their TD origin and development are different, which is another puzzle to be solved.

The expression pattern of Prickle1 in the TD is rather unique. *Prickle1* is found in the growing TD and the mxp epithelium of the NLG and is continuously expressed in the extending TD. This pattern emphasizes a specific need for the function of *Prickle1* during TD development. From initiation to reaching final destinations, the ductal cells maintain epithelial fate (as indicated by E-cadherin expression), but undergo dynamic depolarization, repolarization and intercalation. As a PCP signaling component, *Prickle1* may serve most of these needs because disruption of *Prickle1* alters cell polarity, intercalation and division orientation. It would be highly interesting to know how the spatial and temporal expression of *Prickle1* is determined in cells fated to the TD. As a general principle in developmental biology, positional inductive cues (probably from the maxillary and nasal processes in this case) are probably involved in Prickle1 activation. Additionally, downstream of Prickle1, Fgf/Sox9 appears to play a role in limb growth (Yang et al., 2013). Fgf/Sox9 is also crucial for the development of the ocular glands (Chen et al., 2014). It is likely that Prickle1-regulated PTD growth also involves Fgf signaling, which is another interesting question to be addressed in the future.

Striking cellular changes in the *Prickle1* mutant PTD include disrupted BM deposition and cell-cell adhesion. Basal deposition of BM does not always coincide with adherens junction formation, as observed in both wild-type and mutant PTD. Thus, the data suggest that the function of Prickle1 in BM regulation might be independent of apical cell junctions. On the other hand, the cytoplasmic accumulation of laminin and ectopic deposition of other BM components indicate a misrouted secretory pathway(s). Impaired trafficking does not appear generalized to all proteins because the basal deposition of fibronectin is largely unchanged in the mutant wall cells compared with its wild-type counterpart, and even adherens junctions are not uniformly disrupted. Additionally, coordinated polarization of the Golgi complex and the clathrin-coated vesicles is largely unaffected. Taken together, these data suggest that the trafficking of a select set of proteins (including BM) is altered by the loss of *Prickle1*, consistent with a study reporting that, in *Drosophila*, *prickle* modulates microtubule polarity, impacting axonal vesicle transport (Ehaideb et al., 2014).

PCP crosstalk with the ECM has been demonstrated in axis elongation of multiple organisms, including ascidians (Veeman et al., 2008), flies (Horne-Badovinac, 2014) and frogs (Goto et al., 2005; Dohn et al., 2013). Tubulogenesis driven by PCP has been well studied (Bernascone et al., 2017; Kunimoto et al., 2017), but not from the perspective of ECM contribution. The current study, for the first time, demonstrates the unambiguous role of PCP-controlled ECM secretion in tubulogenesis. Notably, the *Drosophila* egg chamber employs an unusual form of planar polarity with aligned basal actin bundles and BM providing a 'molecular corset' to direct chamber elongation (Horne-Badovinac, 2014). A similar process might also be utilized for PTD elongation to restrict expansive forces and promote lengthening of the duct.

In summary, our study provides first-hand knowledge of the ontogeny of the tear drainage system, which is implicated in a wide range of ocular disorders. Ontogenesis of the TD requires Prickle1-regulated polarized BM secretion and deposition. This process is probably controlled through the role of Prickle1 in directional intracellular trafficking and secretion. Disruption of intrinsic polarized BM secretion ultimately results in an amplified extrinsic impact on apical-basal or tissue polarity.

MATERIALS AND METHODS

Mice and genotyping

Animal husbandry and experimentation were conducted in strict adherence to the Standards in Animal Research: Reporting of In Vivo Experiments (ARRIVE) guidelines, with approval from the Animal Care and Use Committee (ACUC), Zhongshan Ophthalmic Center, Sun Yat-sen University. Mouse strains were originally of mixed genetic backgrounds of C57Bl/6 and Sv129, backcrossed onto C57Bl/6 for many generations (>7), and demonstrated invariable phenotypes. The sex and age of the animals used in each experiment were consistent whenever possible. The sex of embryos did not seem to affect the results of this study and thus were not considered. The *Prickle1* gene-trap mutant strain was created as described previously (Liu et al., 2013, 2014). The straight null allele (*Prickle1*$^{b/+}$) was created by the excision of Cre recombinase driven by the Sox2 promoter (Sox2-Cre) (Liu et al., 2014). Mouse genotyping was conducted as described previously (Liu et al., 2013, 2014). A knock-in

Development (2020) 147, dev191726. doi:10.1242/dev.191726

eYFP reporter under the control of the endogenous *Prickle1* promoter was used to monitor *Prickle1* expression.

Tissues, histology, immunohistochemistry and antibodies

Mice on P1 were sacrificed by decapitation. Dissected mouse heads were directly embedded in OCT (Cat. 4583, Sakura, USA), quickly frozen in liquid nitrogen and stored at −80°C until use.

For collection of timed embryos, the appearance of a vaginal plug was designated as embryonic day 0.5 (E0.5). Embryos of anticipated ages were dissected out of the uterus and fixed in 4% paraformaldehyde for 24 h at 4°C. Samples were washed three times in phosphate-buffered saline (PBS), placed through a series of sucrose solutions (10, 20 and 30%), embedded in OCT and stored at −80°C until use.

For immunostaining, tissue sections were cut at 15 µm (Leica Cryostat 1900), blocked with 10% donkey serum with 0.1% Triton X-100 in PBS (PBST) for 30 min at room temperature, and then incubated with primary antibodies at 4°C overnight. After washing with PBST, sections were incubated with fluorescent dye-conjugated secondary antibodies for 1 h at room temperature (~25°C), washed three times in PBST, and mounted with Fluoromount-G (Southern Biotech, Birmingham, AL).

For vibratome sections, embryos were fixed with 4% PFA, washed with PBS, embedded in 4% agarose and sectioned at 100 µm thickness using the Leica VT 1000S. For immunostaining, sections were incubated with primary antibodies for 24 h in a 48-well culture plate with shaking. After three washes with PBST for 30 min each, sections were incubated with secondary antibodies overnight. Samples were washed three times with PBST (30 min each) and mounted on slides using Fluoromount-G.

For iDISCO (Renier et al., 2014) preparation, the mouse TD at E11 was labeled with p63 antibody. Briefly, embryos were dehydrated through a series of methanol (30, 50, 70, 90 and 100%) after fixation, bleached with H_2O_2/DMSO/methanol (1:1:4), rehydrated through a methanol/PBS series (80, 60, 40, 20 and 0% methanol) and treated with 2% Triton X-100. Embryos were further permeabilized following a published procedure (Renier et al., 2014), blocked with 6% donkey serum and incubated with primary antibody at 37°C for at least 1 day. Embryos were washed in the same incubation buffer for a day (four or five changes of solution), incubated with secondary antibody and washed in the same way as for the primary antibody.

Immunostained embryos were cleared through a methanol series, switched to dichloromethane (DCM, 270997, Sigma) and then to dibenzyl ether (108014, Sigma). The embryos were ready for imaging after clearance.

All antibodies had been extensively used in previous studies, demonstrating consistent localization patterns in immunohistochemistry. Antibodies used in this study were anti-E-cadherin (ab11512, Abcam; 1:500), anti-N-cadherin (QF215275, Life Technologies; 1:500), anti-p63 (ab124762, Abcam; 1:1000), anti-GFP (TP401, Torrey Pines Biolabs; 1:500), anti-GFP (ab6673, Abcam; 1:500), anti-laminin (L9393, Sigma; 1:1000), anti-laminin β1 (ab44941, Abcam; 1:250), anti-collagen IV (ab19808, Abcam; 1:250), anti-Perlecan (MA1-06821, Invitrogen; 1:500), anti-acetylated-tubulin (T6793, Sigma; 1:500), anti-clathrin-H (ab172958, Abcam; 1:250), anti-GRASP65 (ab30315, Abcam; 1:500), AlexaFluor 488-phalloidin (A12379, ThermoFisher; 1:200), AlexaFluor 568-phalloidin (A12380, ThermoFisher; 1:200), anti-integrin α6 (ab105669, Abcam; 1:500), anti-integrin β4 (ab25254, Abcam; 1:500), anti-fibronectin (ab23750, Abcam; 1:500), β-catenin (610153, BD; 1:500), α-catenin (13-9700, ZYMED; 1:500), P120-catenin (66208, Proteintech; 1:500), Ki67 (ab11580; 1:500) and caspase 3 (Cell Signaling, 9664; 1:250).

Imaging and 3D reconstruction

For P1 TD reconstruction, fresh frozen mouse heads were cut coronally at 30 µm and stained with anti-p63 antibody to identify the TD on each section. For embryos from E11 to E14, sections were cut parasagittally at 100 µm and stained with E-cadherin antibody to identify developing TDs.

Fluorescence microscopy images were obtained using a Zeiss confocal microscope (Zeiss LSM880, Zeiss, Oberkochen, Germany) and Imager Z2 equipped with ApoTome (Zeiss, Oberkochen, Germany). Images taken from the microscopes were aligned manually by Photoshop according to the anatomical features of each section. Tear duct structures were traced on each consecutive section and imported to NIH ImageJ software for 3D processing (3D viewer plugins) with the correct image-depth scale, pixel depth and adjusted image coordinates.

Quantification and statistics

Cell axis orientation was quantified by the angle between the apicobasal axis (defined by Grasp65 staining; Fig. 6) and the tubule axis indicated by E-cadherin staining. Similarly, cell division orientation was defined as the angle between the mitotic spindle axis, as indicated by acetylated α-tubulin staining, and the tubule axis. A total of 236 wild-type and 215 mutant cells from 4 animals, and 61 wild-type and 53 mutant cells from 8 animals were quantified for cell axis and cell division orientation, respectively.

Acknowledgements

We thank Dr Tiansen Li from the National Eye Institute for providing valuable suggestions in the preparation of the manuscript. The authors thank Tiansen Li, Rong Ju for critical reading of the manuscript and helpful comments. We thank lab members Shujuan Xu, Shanzhen Peng and Xinyu Gu for technical support.

Competing interests

The authors declare no competing or financial interests.

Author contributions

Formal analysis: R.J.; Investigation: D.G., J.R., F.M., C.L.; Resources: H.O., Y.L.; Data curation: D.G., J.R., K.W., C.L.; Writing - original draft: D.G., J.R., C.L.; Writing - review & editing: C.L.; Supervision: Y.L.; Project administration: F.M.; Funding acquisition: H.O., C.L.

Funding

This work was supported by grants from the National Natural Science Foundation of China (NSFC: 31571077; Beijing, China), the Guangzhou Science and Technology Innovation Center (201707020009; Guangzhou, Guangdong Province, China), '100 People Plan' from Sun Yat-sen University (8300-18821104; Guangzhou, Guangdong Province, China) and research funding from State Key Laboratory of Ophthalmology at Zhongshan Ophthalmic Center (303060202400339; Guangzhou, Guangdong Province, China) to C.L.; and from the National Natural Science Foundation of China (NSFC: 81622012; Beijing, China) to H.O.

Supplementary information

Supplementary information available online at
https://dev.biologists.org/lookup/doi/10.1242/dev.191726.supplemental

Peer review history

The peer review history is available online at
https://dev.biologists.org/lookup/doi/10.1242/dev.191726.reviewer-comments.pdf

References

Allen, R. C. (2014). Hereditary disorders affecting the lacrimal system. *Curr. Opin Ophthalmol.* **25**, 424-431. doi:10.1097/ICU.0000000000000092

Bernascone, I., Hachimi, M. and Martin-Belmonte, F. (2017). Signaling networks in epithelial tube formation. *Cold Spring Harb. Perspect. Biol.* **9**, a027946. doi:10.1101/cshperspect.a027946

Byun, T. H., Kim, J. T., Park, H. W. and Kim, W. K. (2011). Timetable for upper eyelid development in staged human embryos and fetuses. *Anat. Rec.***294**, 789-796. doi:10.1002/ar.21366

Chen, Z., Huang, J., Liu, Y., Dattilo, L. K., Huh, S.-H., Ornitz, D. and Beebe, D. C. (2014). FGF signaling activates a Sox9-Sox10 pathway for the formation and branching morphogenesis of mouse ocular glands. *Development* **141**, 2691-2701. doi:10.1242/dev.108944

de la Cuadra-Blanco, C., Peces-Pena, M. D., Janez-Escalada, L. and Merida-Velasco, J. R. (2006). Morphogenesis of the human excretory lacrimal system. *J. Anat.* **209**, 127-135. doi:10.1111/j.1469-7580.2006.00606.x

Depew, M. J. and Compagnucci, C. (2008). Tweaking the hinge and caps: testing a model of the organization of jaws. *J. Exp. Zool. B Mol. Dev. Evol.* **310B**, 315-335. doi:10.1002/jez.b.21205

Dohn, M. R., Mundell, N. A., Sawyer, L. M., Dunlap, J. A. and Jessen, J. R. (2013). Planar cell polarity proteins differentially regulate extracellular matrix organization and assembly during zebrafish gastrulation. *Dev. Biol.* **383**, 39-51. doi:10.1016/j.ydbio.2013.08.027

Ehaideb, S. N., Iyengar, A., Ueda, A., Iacobucci, G. J., Cranston, C., Bassuk, A. G., Gubb, D., Axelrod, J. D., Gunawardena, S., Wu, C.-F. et al. (2014). prickle modulates microtubule polarity and axonal transport to ameliorate seizures in flies. *Proc. Natl. Acad. Sci. USA* **111**, 11187-11192. doi:10.1073/pnas.1403357111

Ferretti, E., Li, B., Zewdu, R., Wells, V., Hebert, J. M., Karner, C., Anderson, M. J., Williams, T., Dixon, J., Dixon, M. J. et al. (2011). A conserved Pbx-Wnt-p63-Irf6 regulatory module controls face morphogenesis by promoting epithelial apoptosis. *Dev. Cell* **21**, 627-641. doi:10.1016/j.devcel.2011.08.005

Foster, J., II, Kapoor, S., Diaz-Horta, O., Singh, A., Abad, C., Rastogi, A., Moharana, R., Tekeli, O., Walz, K. and Tekin, M. (2014). Identification of an IGSF3 mutation in a family with congenital nasolacrimal duct obstruction. *Clin. Genet.* **86**, 589-591. doi:10.1111/cge.12321

Frame, N. J. and Burkat, C. N. (2009). Identifying an appropriate animal model for the nasolacrimal drainage system. *Ophthalmic Plast Reconstr. Surg.* **25**, 354-358. doi:10.1097/IOP.0b013e3181b30358

Goto, T., Davidson, L., Asashima, M. and Keller, R. (2005). Planar cell polarity genes regulate polarized extracellular matrix deposition during frog gastrulation. *Curr. Biol.* **15**, 787-793. doi:10.1016/j.cub.2005.03.040

Guo, N., Hawkins, C. and Nathans, J. (2004). Frizzled6 controls hair patterning in mice. *Proc. Natl. Acad. Sci. USA* **101**, 9277-9281. doi:10.1073/pnas.0402802101

Horne-Badovinac, S. (2014). The Drosophila egg chamber-a new spin on how tissues elongate. *Integr Comp Biol* **54**, 667-676. doi:10.1093/icb/icu067

Inan, U. U., Yilmaz, M. D., Demir, Y., Degirmenci, B., Ermis, S. S. and Ozturk, F. (2006). Characteristics of lacrimo-auriculo-dento-digital (LADD) syndrome: case report of a family and literature review. *Int. J. Pediatr. Otorhinolaryngol.* **70**, 1307-1314. doi:10.1016/j.ijporl.2005.12.015

Jadico, S. K., Huebner, A., McDonald-McGinn, D. M., Zackai, E. H. and Young, T. L. (2006a). Ocular phenotype correlations in patients with TWIST versus FGFR3 genetic mutations. *J. AAPOS* **10**, 435-444. doi:10.1016/j.jaapos.2006.06.008

Jadico, S. K., Young, D. A., Huebner, A., Edmond, J. C., Pollock, A. N., McDonald-McGinn, D. M., Li, Y.-J., Zackai, E. H. and Young, T. L. (2006b). Ocular abnormalities in Apert syndrome: genotype/phenotype correlations with fibroblast growth factor receptor type 2 mutations. *J. AAPOS* **10**, 521-527. doi:10.1016/j.jaapos.2006.07.012

Kozma, C., Hunt, M., Meck, J., Traboulsi, E. and Scribanu, N. (1990). Familial Wolf-Hirschhorn syndrome associated with Rieger anomaly of the eye. *Ophthalmic Paediatr. Genet.* **11**, 23-30. doi:10.3109/13816819009012945

Kunimoto, K., Bayly, R. D., Vladar, E. K., Vonderfecht, T., Gallagher, A.-R. and Axelrod, J. D. (2017). Disruption of core planar cell polarity signaling regulates renal tubule morphogenesis but is not cystogenic. *Curr. Biol.* **27**, 3120-3131.e4. doi:10.1016/j.cub.2017.09.011

Li, H., Jones, K. L., Hooper, J. E. and Williams, T. (2019). The molecular anatomy of mammalian upper lip and primary palate fusion at single cell resolution. *Development* **146**, dev174888. doi:10.1242/dev.174888

Liu, C., Lin, C., Whitaker, D. T., Bakeri, H., Bulgakov, O. V., Liu, P., Lei, J., Dong, L., Li, T. and Swaroop, A. (2013). Prickle1 is expressed in distinct cell populations of the central nervous system and contributes to neuronal morphogenesis. *Hum. Mol. Genet.* **22**, 2234-2246. doi:10.1093/hmg/ddt075

Liu, C., Lin, C., Gao, C., May-Simera, H., Swaroop, A. and Li, T. (2014). Null and hypomorph Prickle1 alleles in mice phenocopy human Robinow syndrome and disrupt signaling downstream of Wnt5a. *Biol. Open* **3**, 861-870. doi:10.1242/bio.20148375

Lotz, K., Proff, P., Bienengraeber, V., Fanghaenel, J., Gedrange, T. and Weingaertner, J. (2006). Apoptosis as a creative agent of embryonic development of bucca, mentum and nasolacrimal duct. An in vivo study in rats. *J. Craniomaxillofac. Surg.* **34** Suppl. 2, 8-13. doi:10.1016/S1010-5182(06)60003-6

Nowack, C. and Wöhrmann-Repenning, A. (2010). The nasolacrimal duct of anuran amphibians: suggestions on its functional role in vomeronasal perception. *J. Anat.* **216**, 510-517. doi:10.1111/j.1469-7580.2009.01208.x

Paulsen, F. P., Foge, M., Thale, A. B., Tillmann, B. N. and Mentlein, R. (2002a). Animal model for the absorption of lipophilic substances from tear fluid by the epithelium of the nasolacrimal ducts. *Invest. Ophthalmol. Vis. Sci.* **43**, 3137-3143.

Paulsen, F., Thale, A. and Schaudig, U. (2002b). [Nasolacrimal ducts and the dry eye]. *Ophthalmologe* **99**, 566-574. doi:10.1007/s00347-001-0585-6

Paulsen, F., Garreis, F., Schicht, M., Bräuer, L., Ali, M. J. and Sel, S. (2016). [Anatomy and physiology of the nasolacrimal ducts]. *HNO* **64**, 354-366. doi:10.1007/s00106-016-0164-4

Pearson, A. A. (1980). The development of the eyelids. Part I. External features. *J. Anat.* **130**, 33-42.

Rehorek, S. J., Holland, J. R., Johnson, J. L., Caprez, J. M., Cray, J., Mooney, M. P., Hillenius, W. J. and Smith, T. D. (2011). Development of the lacrimal apparatus in the rabbit (Oryctolagus cuniculus) and its potential role as an animal model for humans. *Anat. Res. Int.* **2011**, 623186. doi:10.1155/2011/623186

Rehorek, S. J., Cunningham, J., Bruening, A. E., Johnson, J. L., Bhatnagar, K. P., Smith, T. D. and Hillenius, W. J. (2015). Development of the nasolacrimal apparatus in the Mongolian gerbil (Meriones unguiculatus), with notes on network topology and function. *J. Morphol.* **276**, 1005-1024. doi:10.1002/jmor.20393

Renier, N., Wu, Z., Simon, D. J., Yang, J., Ariel, P. and Tessier-Lavigne, M. (2014). iDISCO: a simple, rapid method to immunolabel large tissue samples for volume imaging. *Cell* **159**, 896-910. doi:10.1016/j.cell.2014.10.010

Rohmann, E., Brunner, H. G., Kayserili, H., Uyguner, O., Nürnberg, G., Lew, E. D., Dobbie, A., Eswarakumar, V. P., Uzumcu, A., Ulubil-Emeroglu, M. et al. (2006). Mutations in different components of FGF signaling in LADD syndrome. *Nat. Genet.* **38**, 414-417. doi:10.1038/ng1757

Rossie, J. B. and Smith, T. D. (2007). Ontogeny of the nasolacrimal duct in primates: functional and phylogenetic implications. *J. Anat.* **210**, 195-208. doi:10.1111/j.1469-7580.2006.00682.x

Ru, J., Guo, D., Fan, J., Zhang, J., Ju, R., Ouyang, H., Wei, L., Liu, Y. and Liu, C. (2020). Malformation of tear ducts underlies the epiphora and precocious eyelid opening in Prickle1 mutant mice: genetic implications for tear duct genesis. *Invest. Ophthalmol. Vis. Sci.* **61**, 6. doi:10.1167/iovs.61.13.6

Saburi, S., Hester, I., Fischer, E., Pontoglio, M., Eremina, V., Gessler, M., Quaggin, S. E., Harrison, R., Mount, R. and McNeill, H. (2008). Loss of Fat4 disrupts PCP signaling and oriented cell division and leads to cystic kidney disease. *Nat. Genet.* **40**, 1010-1015. doi:10.1038/ng.179

Sanchez-Tena, M. A. M. A., Alvarez-Peregrina, C. C. and Villa-Collar, C. C. (2019). Dry eye analysis: a citation network study. *J. Ophthalmol.* **2019**, 3048740. doi:10.1155/2019/3048740

Sevel, D. (1988). A reappraisal of the development of the eyelids. *Eye (Lond)* **2**, 123-129. doi:10.1038/eye.1988.25

Tamarin, A. and Boyde, A. (1977). Facial and visceral arch development in the mouse embryo: a study by scanning electron microscopy. *J. Anat.* **124**, 563-580.

Tawfik, H. A., Abdulhafez, M. H., Fouad, Y. A. and Dutton, J. J. (2016). Embryologic and fetal development of the human eyelid. *Ophthalmic Plast. Reconstr. Surg.* **32**, 407-414. doi:10.1097/IOP.0000000000000702

Vagge, A., Ferro Desideri, L., Nucci, P., Serafino, M., Giannaccare, G., Lembo, A. and Traverso, C. E. (2018). Congenital Nasolacrimal Duct Obstruction (CNLDO): A Review. *Diseases* **6**, 96. doi:10.3390/diseases6040096

van Genderen, M. M., Kinds, G. F., Riemslag, F. C. and Hennekam, R. C. (2000). Ocular features in Rubinstein-Taybi syndrome: investigation of 24 patients and review of the literature. *Br. J. Ophthalmol.* **84**, 1177-1184. doi:10.1136/bjo.84.10.1177

Veeman, M. T., Nakatani, Y., Hendrickson, C., Ericson, V., Lin, C. and Smith, W. C. (2008). Chongmague reveals an essential role for laminin-mediated boundary formation in chordate convergence and extension movements. *Development* **135**, 33-41. doi:10.1242/dev.010892

Wallace, E. J., Cox, A., White, P. and Macewen, C. J. (2006). Endoscopic-assisted probing for congenital nasolacrimal duct obstruction. *Eye* **20**, 998-1003. doi:10.1038/sj.eye.6702049

Wallingford, J. B. and Harland, R. M. (2002). Neural tube closure requires Dishevelled-dependent convergent extension of the midline. *Development* **129**, 5815-5825. doi:10.1242/dev.00123

Wallingford, J. B., Fraser, S. E. and Harland, R. M. (2002). Convergent extension: the molecular control of polarized cell movement during embryonic development. *Dev. Cell* **2**, 695-706. doi:10.1016/S1534-5807(02)00197-1

Wang, Y., Guo, N. and Nathans, J. (2006). The role of Frizzled3 and Frizzled6 in neural tube closure and in the planar polarity of inner-ear sensory hair cells. *J. Neurosci.* **26**, 2147-2156. doi:10.1523/JNEUROSCI.4698-05.2005

Yang, T., Bassuk, A. G. and Fritzsch, B. (2013). Prickle1 stunts limb growth through alteration of cell polarity and gene expression. *Dev. Dyn.* **242**, 1293-1306. doi:10.1002/dvdy.24025

Yu, H., Ye, X., Guo, N. and Nathans, J. (2012). Frizzled 2 and frizzled 7 function redundantly in convergent extension and closure of the ventricular septum and palate: evidence for a network of interacting genes. *Development* **139**, 4383-4394. doi:10.1242/dev.083352